Electronic Supplementary Material (ESI) for Energy & Environmental Science.

ELECTRONIC SUPPLEMENTARY INFORMATION

Selective CO production from aqueous CO_2 using a $Cu_{96}In_4$ catalyst and its integration into a bias-free solar perovskite-$BiVO_4$ tandem device

Motiar Rahaman,[1] Virgil Andrei,[1] Chanon Pornrungroj,[1] Demelza Wright,[1,2] Jeremy J. Baumberg,[2] and Erwin Reisner[1,*]

[1]*Department of Chemistry, University of Cambridge, Lensfield Road, Cambridge CB2 1EW, United Kingdom*

[2]*NanoPhotonics Centre, Cavendish Laboratory, Department of Physics, University of Cambridge, J J Thomson Avenue, Cambridge CB3 0HE, United Kingdom*

***Corresponding author**

Prof. Erwin Reisner

Postal address: *Department of Chemistry, University of Cambridge, Lensfield Road, Cambridge CB2 1EW, UK*

E-mail: reisner@ch.cam.ac.uk

Tel: +44-1223336323

Website: http://www-reisner.ch.cam.ac.uk

MATERIALS AND CHEMICALS

Catalyst preparation. Copper(II) sulfate pentahydrate ($CuSO_4 \cdot 5H_2O$, 99.995%), indium(III) sulfate hydrate ($In_2(SO_4)_3 \cdot xH_2O$, 99.99%), and suprapur sulfuric acid (H_2SO_4, 96%) were purchased from Sigma Aldrich, Cu foil (99.9%) from Alfa Aesar, orthophosphoric acid (H_3PO_4, 68%) was purchased from Fluka.

Perovskite and $BiVO_4$ deposition. Conductive FTO glass substrate (~7Ω sq^{-1}), $Ni(NO_3)_2 \cdot 6H_2O$ (≥98.5%), DMF (anhydrous, 99.8%), polyethylenimine (PEIE, 80% ethoxylated solution, 35–40 wt% in H_2O, average M_w 70,000), poly(triarylamine) (PTAA), F4TCNQ (97%) H_2O_2 solution (30%), and graphite powder were purchased from Sigma-Aldrich. Ethylene glycol (99.8%, anhydrous), 1-methyl-2-pyrrolidone (99.5%, extra dry over molecular sieves), chloroform (99.9%, extra dry over molecular sieves), Zn (dust, 98+%), and chlorobenzene (extra dry over molecular sieves ≥99.5%), were purchased from ACROS. Perovskite precursors PbI_2 (99.99%,), and $PbBr_2$ were purchased from TCI, formamidinium iodide, methylammonium bromide were purchased from Dyesol. Ethylenediamine (absolute, ≥99.5%), and HCl (reagent grade) were purchased from Fluka. DMF (99%), dimethyl sulfoxide (ACS reagent, ≥99.9% and 99+%) were purchased from Alfa Aesar, analytical reagent grade chloroform, acetonitrile (HPLC grade). NaI (laboratory reagent grade) were purchased from Fischer Scientific, [6,6]-phenyl C61 butyric acid methyl ester (PCBM, 99%) was purchased from Solenne BV. Isopropanol (≥99.5%) was purchased from Honeywell.

$Bi(NO_3)_3 \cdot 5H_2O$ (98%) was purchased from Sigma-Aldrich, vanadyl acetylacetonate (≥97.0%) was purchased from Fluka, NaOH (analytical reagent grade) was purchased from Fischer Scientific.

Electrochemical / photoelectrochremical experiments. ACS reagent grade $KHCO_3$ (≥99.7%) was purchased from Sigma Aldrich.

All the chemicals were used as purchased without further purification.

METHODS

Synthesis of the catalyst.

The Cu_xIn_y alloy catalysts were synthesized via a template assisted electrodeposition method following previously reported protocols.[1, 2] Cu foil was used as substrate for electrodeposition. Prior to electrodeposition, the substrates were electropolished in 50% ortho-phosphoric acid by applying +2.0 V for 90 s.

The electrodeposition of the bimetallic material was conducted in a clean glass beaker containing copper sulfate and indium sulfate precursor salts (0.025 M) in 1.5 M sulfuric acid solution. Different ratios of precursor salts were used to vary the metal composition in the alloy. A three-electrode set-up was used where the Cu foil substrate was used as working electrode, a Cu foil (4 x 4 cm) as the counter electrode and a leak-free Ag/AgCl (saturated NaCl, BASI) electrode as the reference electrode. For the galvanostatic deposition process, a current density of $j = -3.0$ A cm^{-2} was applied for 60 s. After electrodeposition, the catalysts were cleaned by dipping into Milli-Q water for 120 s and dried under N_2 stream at room temperature.

Deposition of inverse structure perovskite. Inverse structure triple cation mixed halide perovskite photovoltaic cells were prepared by adapting a previously reported method.[3] A NiO_x hole transport layer (HTL) was deposited on the FTO-coated glass by spin coating a 1.0 M $Ni(NO_3)_2 \cdot 6H_2O$, 1.0 M ethylenediamine solution in ethylene glycol followed by an annealing treatment at 573 K. Then the samples were transferred into a glovebox, where PTAA doped with F4TCNQ was spin coated as a second HTL. A cesium formamidinium methylammonium (CsFAMA) perovskite precursor solution was prepared by first preparing 1000 µL of a $FAMA_{0.22}Pb_{1.32}I_{3.2}Br_{0.66}$ solution in 510 µL of DMF, 340 µL of DMSO and 150 µL of NMP, followed by addition of 48 µL of 1.5 M CsI in DMSO. The perovskite solution was then spin coated onto the PTAA:F4TCNQ layer in two steps; first 10 s at 1000 rpm and then 35 s at 6000 rpm using chloroform as the antisolvent ~7 s before the end of spin coating. The perovskite layer was then

annealed at 373 K for 30 min. The perovskite layer appeared as a transparent black film on top of the substrate. Then, a thin [6,6]-phenyl C61 butyric acid methyl ester (PCBM) electron transport layer was deposited on top of the perovskite filmby spin coating 35 mg mL^{-1} PCBM solution in chlorobenzene at 3000 rpm for 45 s. A PEIE film was also deposited on top of the PCBM coated perovskite layer by spin coating 3.87 µL mL^{-1} PEIE solution in IPA at 3000 rpm for 30 s to prevent interfacial degradation by reacting with the metal contact. A conductive silver layer was deposited by metal evaporation as electrical contact between the perovskite and the encapsulating graphiteepoxy. The 100 nm Ag layer was deposited in such a way that the active perovskite area becomes around ~0.5 x 0.5 cm. All the photovoltaic cells used in this study have an active area between 0.225 to 0.275 cm^2.

Preparation of $BiVO_4$|TiCo photoanode. $BiVO_4$ photoanodes were prepared following a reported procedure.[3, 4] At first BiOI was electrodeposited onto an FTO substrate (with a defined exposed active area) from a precursor solution prepared by adding 20 mL of a 0.02 M $Bi(NO_3)_3 \cdot 5H_2O$, 0.4 M NaI aqueous solution to 9 mL of a 0.3 M benzoquinone solution in ethanol. The electrodeposition was carried out by applying –0.3 V vs Ag/AgCl for 5 s and then –0.1 V vs Ag/AgCl for 180 s. Then, 40 µL cm^{-2} of a 0.4 M $VO(acac)_2$ solution was dropcast onto the electrodeposited BiOI, followed by annealing of the samples at 723 K for 1 h to form the $BiVO_4$ photoanodes. The prepared samples were stirred in 0.2 M NaOH solution to dissolve excess V_2O_5 from the $BiVO_4$ surface. Finally, an amorphous TiCo oxide catalyst was deposited on the surface by spin coating 20 µL cm^{-2} of a 4.8 mg mL^{-1} $[Ti_4O(OEt)_{15}(CoCl)]$ solution (in dry toluene) at 2000 rpm for 10 s under air to form the active $BiVO_4$|TiCo photoanode.[3]

Preparation of perovskite|Cu_xIn_y cathodes by conductive epoxy encapsulating layer. A conductive epoxy paste was prepared by homogeneously mixing graphite power with epoxy (Araldite Standard 2 component epoxy) in a 3:4 mass ratio of graphite:epoxy.[5] The catalyst was interfaced to the device with the help of the paste. The device was kept overnight to harden the

conductive epoxy paste. Finally, a wire was connected to the FTO glass with conductive Ag paste and the device edges were encapsulated by Araldite 5-Minute Rapid epoxy.

Assembly of the tandem device. The $BiVO_4$ photoanode was also encapsulated by epoxy after attaching a connecting wire with the help of conducting Ag paste. For an artificial leaf-type tandem assembly the perovskite|$Cu_{96}In_4$ cathode and the $BiVO_4$ photoanode were attached to each other by epoxy glue. To prevent excess photoabsorption, the inactive area of the $BiVO_4$-TiCo phonoanode was covered by black tape. The active surface areas of perovskite, $BiVO_4$, and catalyst were measured before the assembly.

PEC and EC measurements and product quantification. A certified Newport 1916-R optical power meter was used to calibrate the Newport Oriel 67005 solar light simulator with Air Mass 1.5 Global (AM 1.5G) solar filters to 100 mW cm^{-2} (1 Sun) prior to each PEC experiment. The lower light intensities were obtained by additionally employing neutral density filters with 50% and 20% transmission. All electrochemical and PEC experiments were conducted with a PalmSens Multi $EmStat^{3+}$ (multichannel potentiostat consisting of four separate channels) and Ivium CompactStat potentiostats. The reaction medium was an aqueous 0.5 M $KHCO_3$ solution, which was purged for at least 30 min prior to the experiments with CO_2 or N_2 (with 2% methane internal standard). A three-electrode set up consisting of a Ag/AgCl (sat. NaCl) (BasiMW-2030) reference, a platinum mesh counter, and a Cu_xIn_y or a perovskite|Cu_xIn_y working electrode was used in a two-compartment gas tight cell for the electrochemical and PEC measurements. PEC measurements were performed under chopped light irradiation (50 min on, 10 min off). All the experiments were carried out at room temperature. A Selemion (AGC Engineering) anion exchange membrane was used to separate the cathode and anode compartments. An additional EC experiment was carried out with an ultrapure $KHCO_3$ which was prepared by purging CO_2 through 99.995% K_2CO_3 solution and then further purified by soaking for at least 24 h in regenerated Chelex 100 sodium form resin

(50-100 mesh (dry), Sigma Aldrich) to test for any effects from trace amounts of heavy metal ions (which might be present in the as-purchased electrolyte) on the catalytic activity of $Cu_{96}In_4$ material (Fig. S19).[6] All potentials measured with respect to the Ag/AgCl reference were converted to the reversible hydrogen scale using the equation E (V vs. RHE) = E (V vs. Ag/AgCl) + 0.059 V x pH + 0.197 V at 298 K.

The bias-free PEC experiments were carried out using a tandem device assembled in a back to back artificial leaf configuration, in a one compartment cell using CO_2 saturated aqueous 0.5 M $KHCO_3$ (pH 7.2) at room temperature. To avoid any aerobic leakage, O_2 quantification experiments were performed inside a UniLab glovebox under an inert atmosphere. The photoanodic O_2 evolution was monitored by a NeoFox-GT fluorometer and Fospor-R fluorescence oxygen sensor probe from Ocean Optics (see Fig. S20 for more details about the O_2 analysis). CO and H_2 from the perovskite|$Cu_{96}In_4$ cathode were quantified by manual injection from the headspace of the PEC cell into a Shimadzu GC-2010 Plus gas chromatograph (GC). After the experiment, the electrolyte solution was analyzed by ^{1}H NMR spectroscopy (Bruker 400 MHz, sodium 3-(trimethylsilyl)propionate was used as internal standard) and by ion exchange chromatography (Metrohm 882 IC Plus) to investigate the presence of any liquid products.

The lower total faradaic efficiency at the beginning of the experiment was presumably due to bubble trapping inside the porous catalyst architecture, and solubilized gaseous products inside the electrolyte solution. With time, the concentration of the gaseous products increases into the headspace, thus the total product efficiency is close to 100%.

The solar-to-fuel efficiency (STF). The solar-to-CO (STC) efficiency was calculated using the following equation[7]

$$\text{STC} = \frac{|\ \text{Photocurrent density (mA cm}^{-2})\ |\ 1.34\ (V)\ FE_{CO}}{\text{P (mW cm}^{-2})}$$

On the other hand, solar-to-H_2 (STH) efficiency was calculated using the equation[8]

$$\text{STH} = \frac{\text{Photocurrent density (mA cm}^{-2}\text{)} \times 1.23\ (V)\ \text{FE}_{H2}}{\text{P (mW cm}^{-2}\text{)}}$$

Operando **Raman spectroscopy.** Measurements were recorded on a modified Olympus BX51 coupled to a 633 nm laser. Excitation and collection were through a 0.25 NA 10× Olympus objective. Spectra were recorded by an Andor camera coupled to a Triax 550 spectrometer. A specially designed three-electrode cell is used. A platinum mesh (Alfa Aesar) is used for counter electrode, and Ag/AgCl (3 M KCl, eDAQ ET072, Green Leaf Scientific) as reference electrode. The cell is closed by a 25 × 25 × 0.2 mm glass cover slip. Electrochemical measurements were recorded on an Autolab PGSTAT204 (Metrohm).

Material Characterization. A TESCAN MIRA3 FEG-SEM instrument equipped with an Oxford Instruments Aztec Energy X-maxN 80 EDX system was used for the SEM, HR-SEM and EDX analysis. The TEM measurements, STEM mappings, and high-resolution point EDX analysis were carried out by a Thermo Scientific Talos F200X G2 TEM (FEI, operating voltage 200kV). XPS analysis was performed at the Maxwell Center (University of Cambridge) with a near ambient pressure (NAP) X-ray photoemission spectroscopy (XPS) system which uses a SPECS XR 50 MF X-ray Source, µ-FOCUS 600 X-ray monochromator and differentially pumped PHOIBOS 150 1D-DLD NAP analyzer. Powder X-ray diffraction was performed by a Panalytical X'Pert Pro (K alpha Cu radiation) diffractometer from 2Θ 20° to 80°. ICP-OES measurements were performed at the Microanalysis Service, Department of Chemistry, University of Cambridge on a Thermo Scientific iCAP 7400 ICP-OES DUO spectrometer.

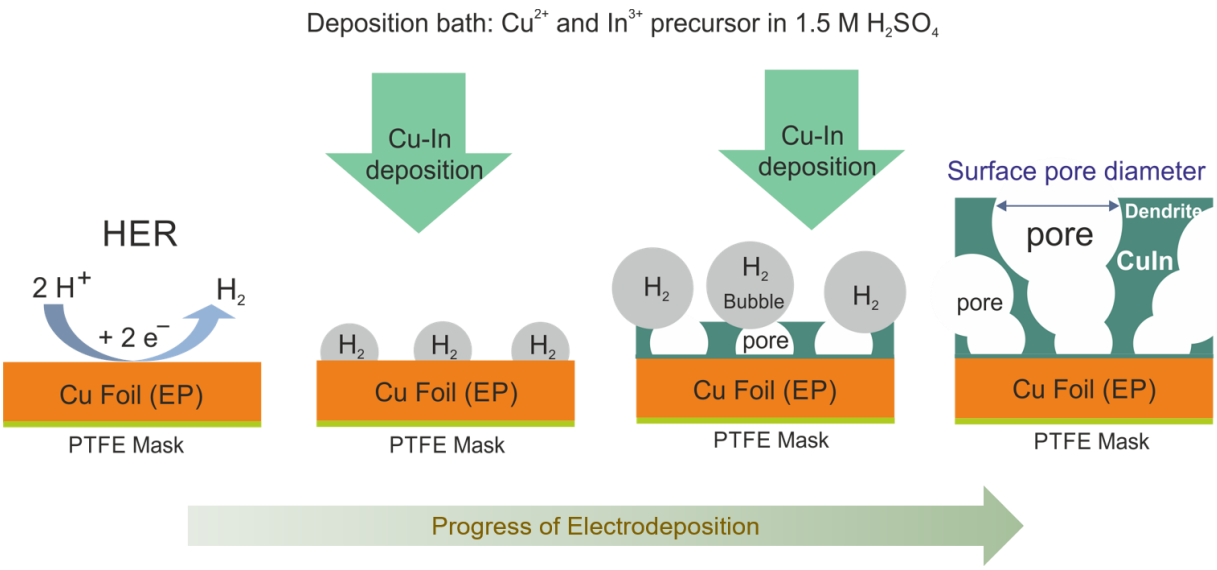

Fig. S1 Schematic representation of the template assisted electrodeposition process showing H_2 bubbles acting as a template for making the mesoporous architecture of the catalyst. HER: hydrogen evolution reaction, EP: electropolished, PTFE: polytetrafluoroethylene (Teflon). The scheme has been adopted from ref. 2.

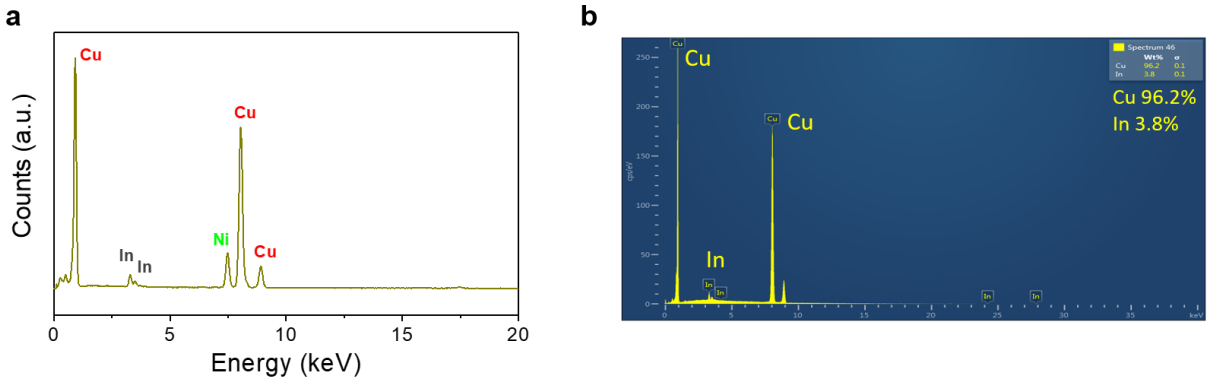

c

Method	Cu [%]	In [%]
ICP-OES	96.06	3.94
SEM-EDX	96.4±0.3	3.6±0.3
TEM-EDX	95.8±0.4	4.2±0.4

Fig. S2 Elemental analysis: EDX spectra taken in (a) TEM mode and (b) SEM mode, (c) a table showing Cu and In percentage in the as prepared catalyst material from the ICP-OES, SEM EDX, and TEM EDX analysis.

.

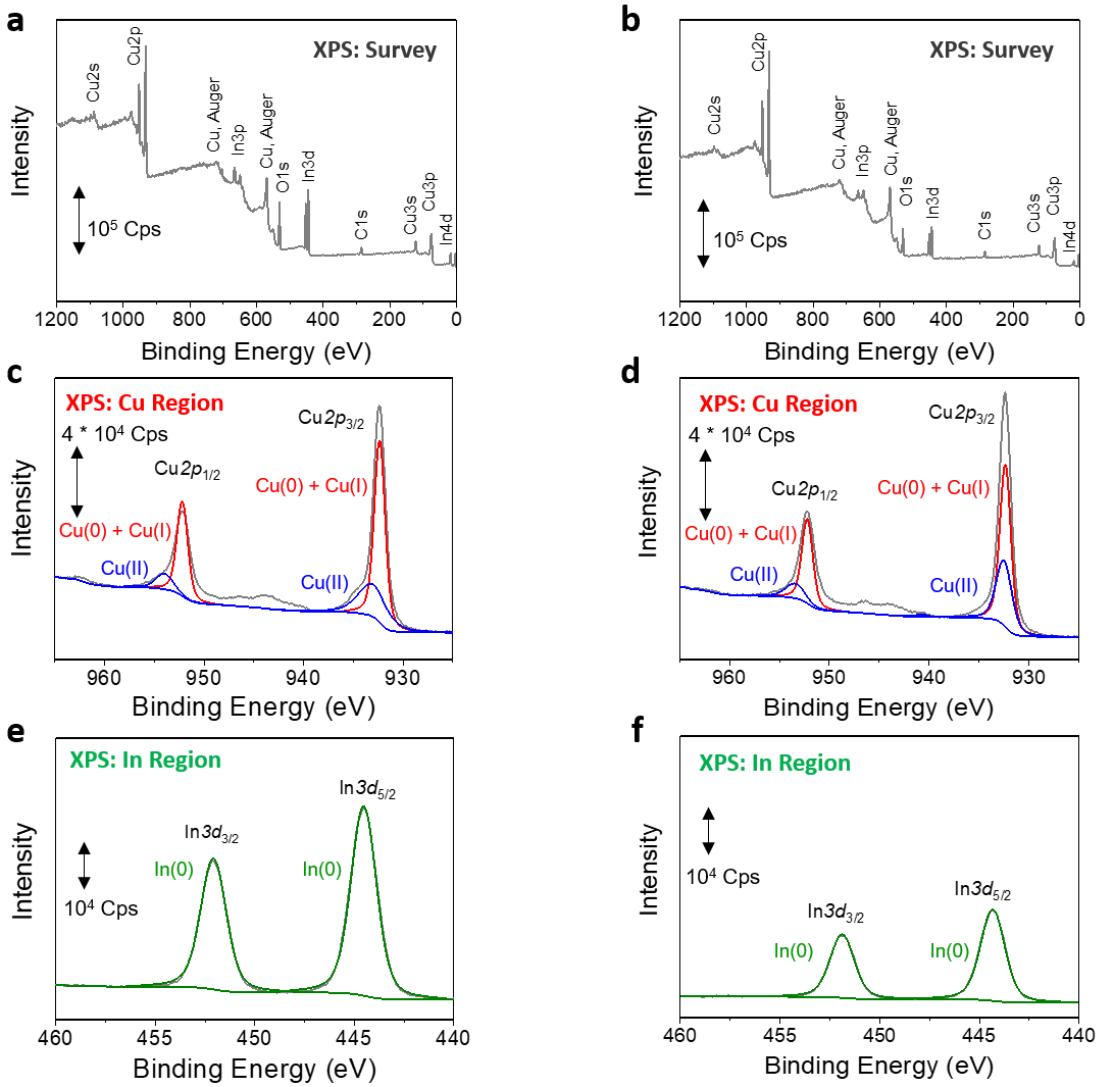

Fig. S3 XPS analysis with the as prepared $Cu_{96}In_4$ catalysis (left column; a,c,e) showing the survey, Cu2p, and In3d regions. The right column (b, d, f) shows the same for a $Cu_{96}In_4$ catalyst after 10 h bias-free PEC experiment. The initial ratio of (Cu + Cu_xO) and In components was 88 : 12 on the surface of the as-prepared catalyst. After the experiment, the ratio becomes 93 : 7. The decrease of about 40% in the In percentage supports the migration of the In phase from the surface to the bulk over the course of the experiment. Note that the surface elemental ratio from the surface-sensitive XPS analysis differs from the actual bulk composition determined by the EDX and ICP-OES analysis.

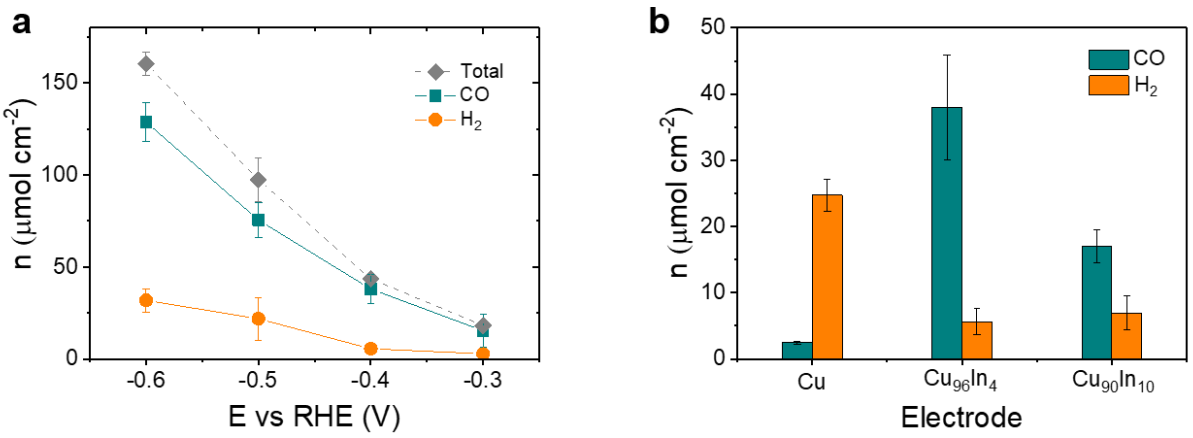

Fig. S4 Amounts of gaseous products formed in electrochemical CO_2 conversion. (a) $Cu_{96}In_4$ catalyst at different applied potentials, and (b) at –0.4V vs RHE using catalysts with different compositions. CO_2 saturated 0.5 M aqueous $KHCO_3$ was used as the electrolyte solution. Electrolysis duration was 4 h. All experiments were carried out at room temperature.

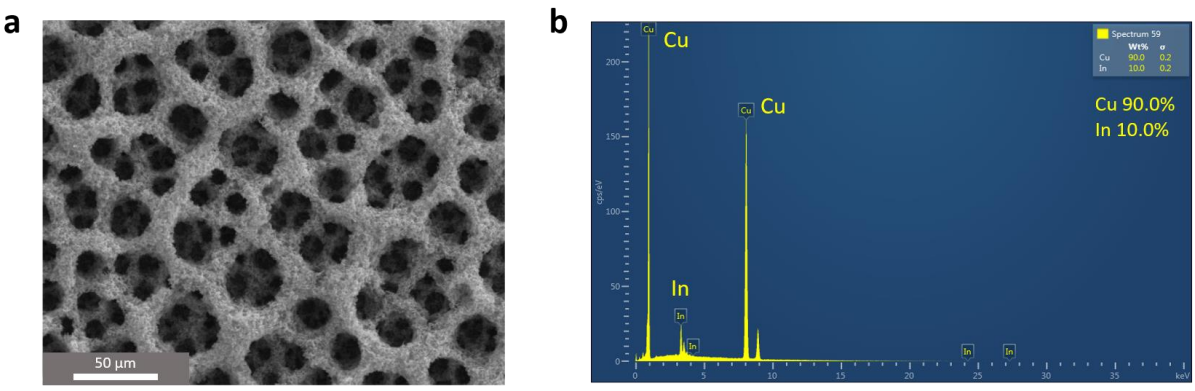

Fig. S5 (a) SEM and (b) EDX analysis of the alloy with higher In content. From the EDX elemental analysis, the material was named $Cu_{90}In_{10}$.

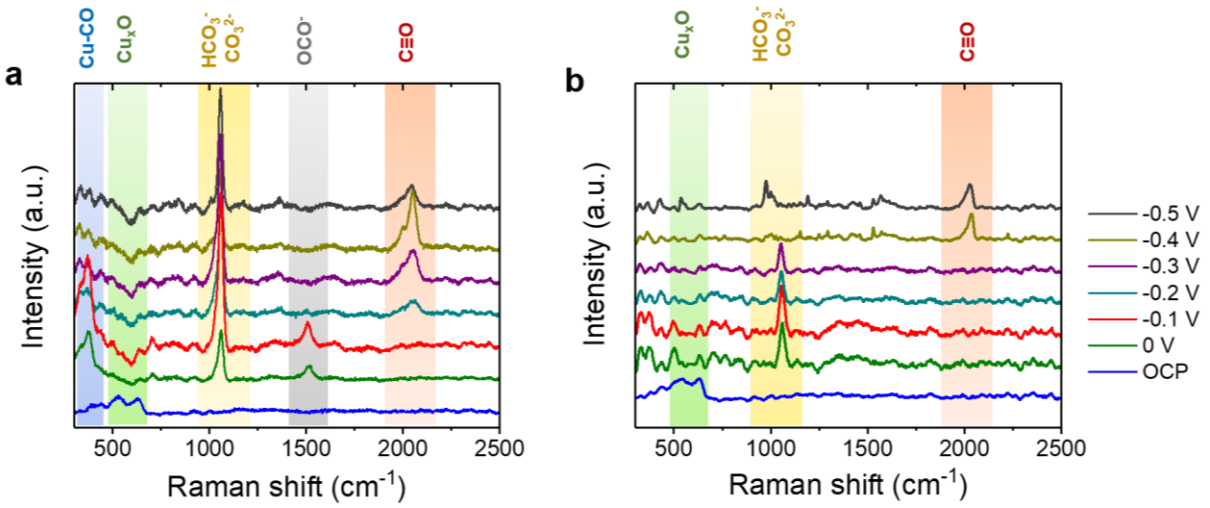

Fig. S6 Full range operando Raman spectra of (a) pristine Cu foam and (b) $Cu_{96}In_4$ alloy foam in CO_2 saturated 0.5 M aqueous $KHCO_3$ solution (pH 7.2). The carbonate / bicarbonate adsorption peaks can be observed along with the adsorbed C≡O peaks. Note that the Cu_xO peaks at 500 to 700 cm^{-1} range can be observed for both samples at OCP and they disappear after a cathodic potential has been applied. This suggests that the surface oxides are unstable under the cathodic environment and they are reduced to the metallic phase when the negative potential is applied. The spectro-electrochemistry was performed in a three-electrode configuration using a 633 nm laser. The experiments were carried out at room temperature.

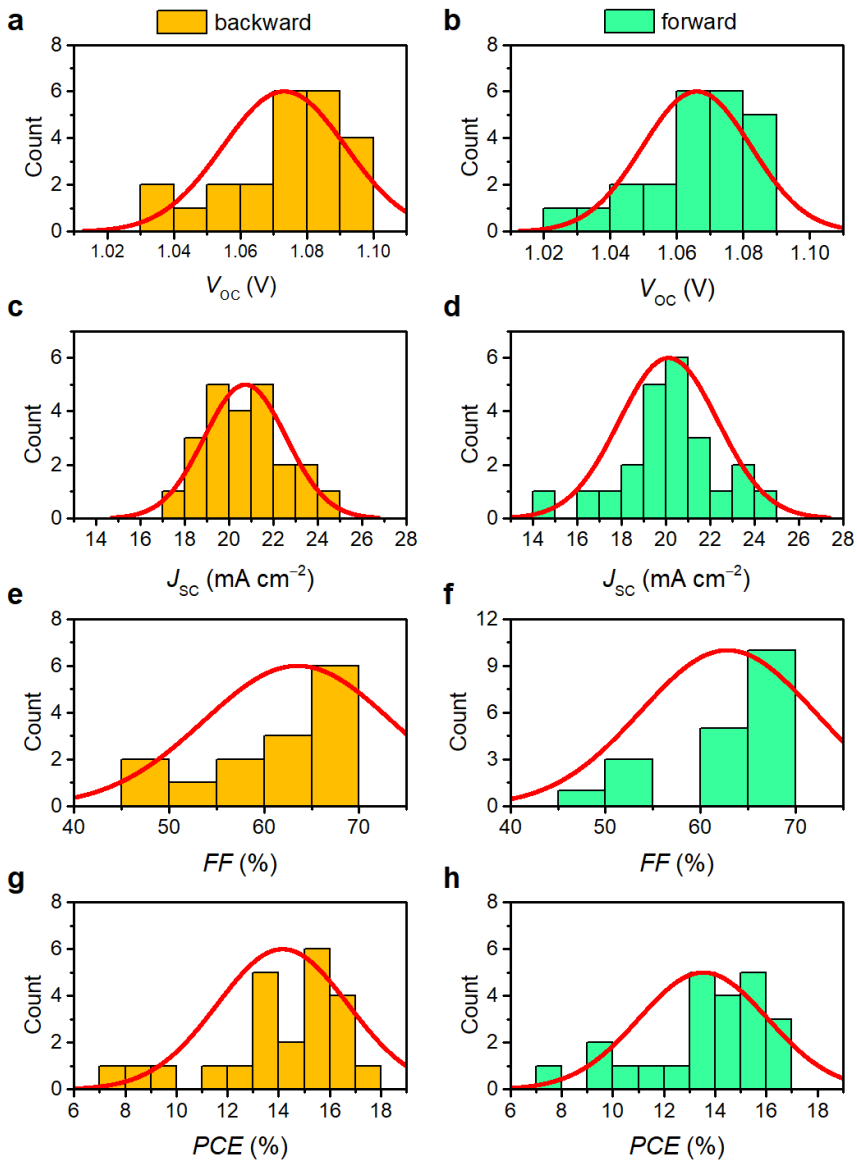

Fig. S7 The histograms of the photovoltaic parameters are depicted in orange for the backward scans (a,c,e,g) and green for the forward scans (b,d,f,h): (a,b) open circuit voltage (V_{OC}), (c,d) short circuit current density (J_{SC}), (e,f) fill factor (*FF*), and (g,h) photovoltaic cell efficiency (*PCE*). The red lines indicate the normal distribution curves. The devices with a NiO_x|PTAA HTL average 1.07 ± 0.02 V V_{OC}, −20.7 ± 1.8 mA cm^{-2} J_{SC}, 63.5 ± 9.9% *FF*, 14.1 ± 2.6% PCE in backward scan, and 1.07 ± 0.02 V V_{OC}, −20.1 ± 2.2 mA cm^{-2} J_{SC}, 62.8 ± 9.2% *FF*, 13.5 ± 2.5% *PCE* in forward scan direction.

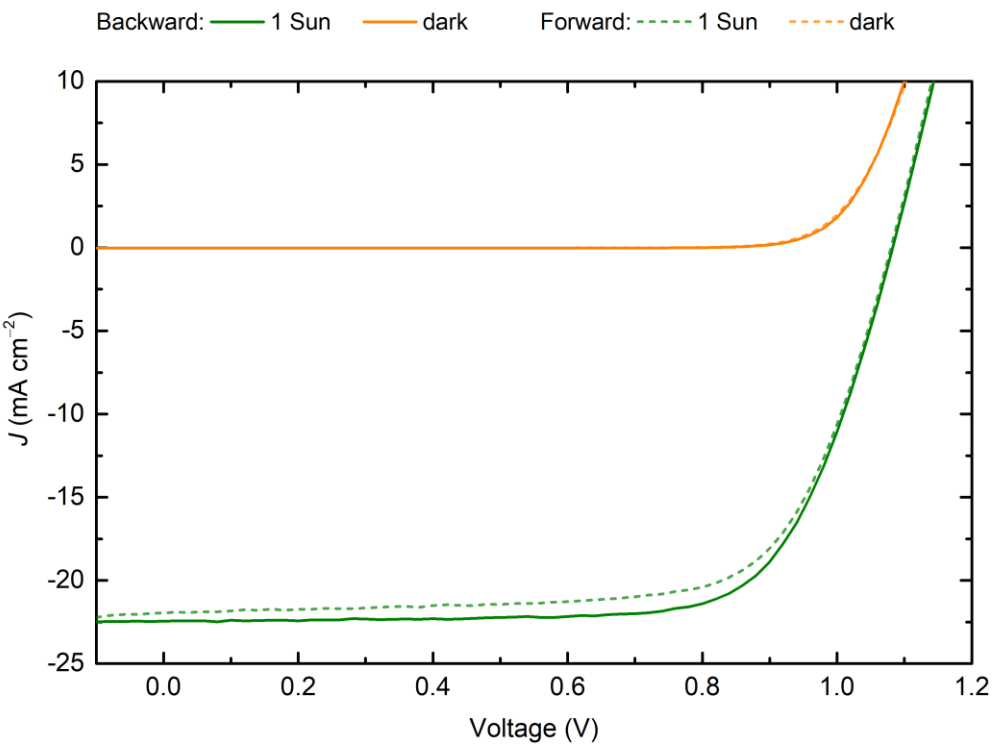

Fig. S8 Light and dark J-V curves of the champion perovskite PV device, in forward and backward scan. The device reaches 1.082 V V_{OC}, −22.5 mA cm^{-2} J_{SC}, 71.9% *FF*, 17.5% *PCE* in backward scan direction.

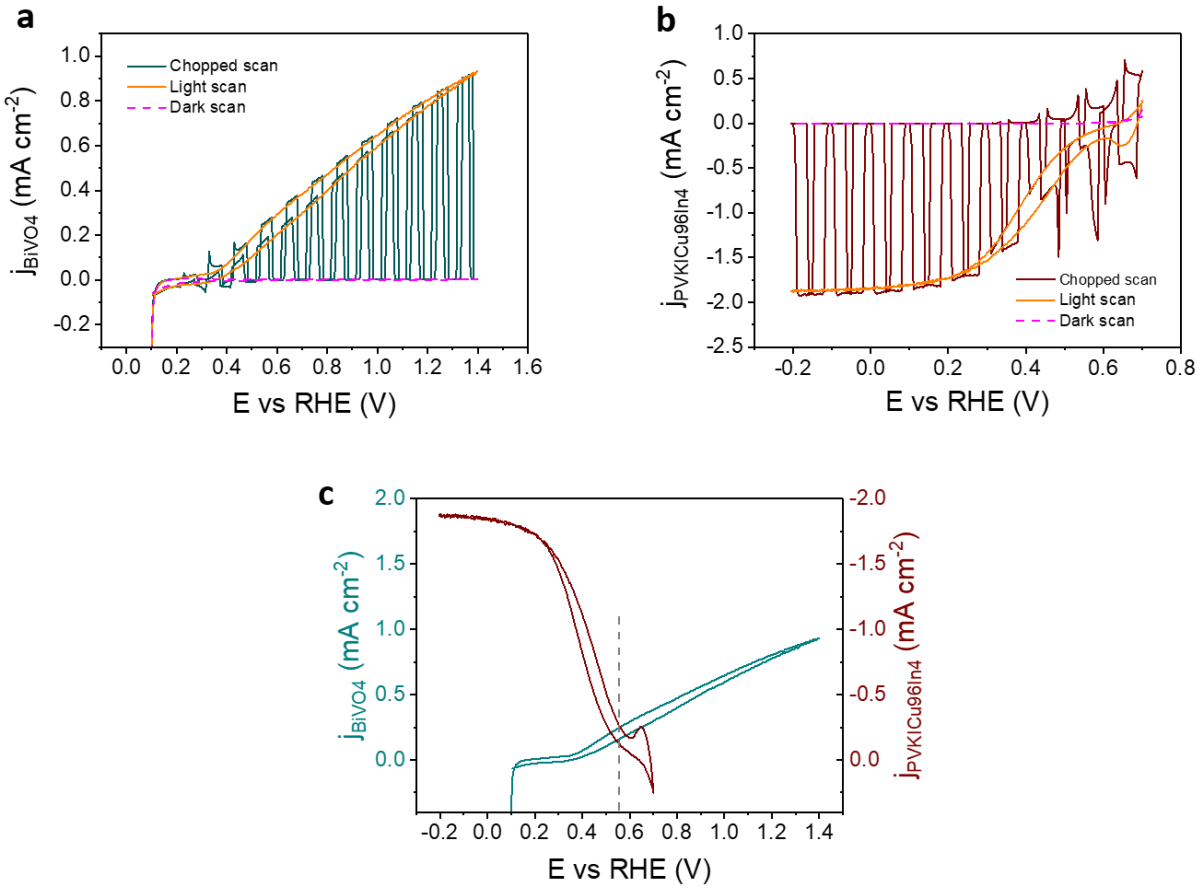

Fig. S9 $BiVO_4$||perovskite|$Cu_{96}In_4$ tandem assembly. (a) CV scan of the $BiVO_4$ photoanode, (b) CV scan of perovskite|$Cu_{96}In_4$ cathode behind the $BiVO_4$ photoanode under chopped, continuous, and no artificial sunlight illumination (1 Sun, AM1.5G, 100 mW cm^{-2}, scan rate 10 mV s^{-1}). (c) Overlap of $BiVO_4$ and PVK CVs under continuous light irradiation. The two curves overlap at +0.55V vs RHE and show a photocurrent ~208 mA cm^{-2}. The CVs were taken in CO_2 saturated aqueous 0.5 M aqueous $KHCO_3$ solution (pH 7.2) at room temperature.

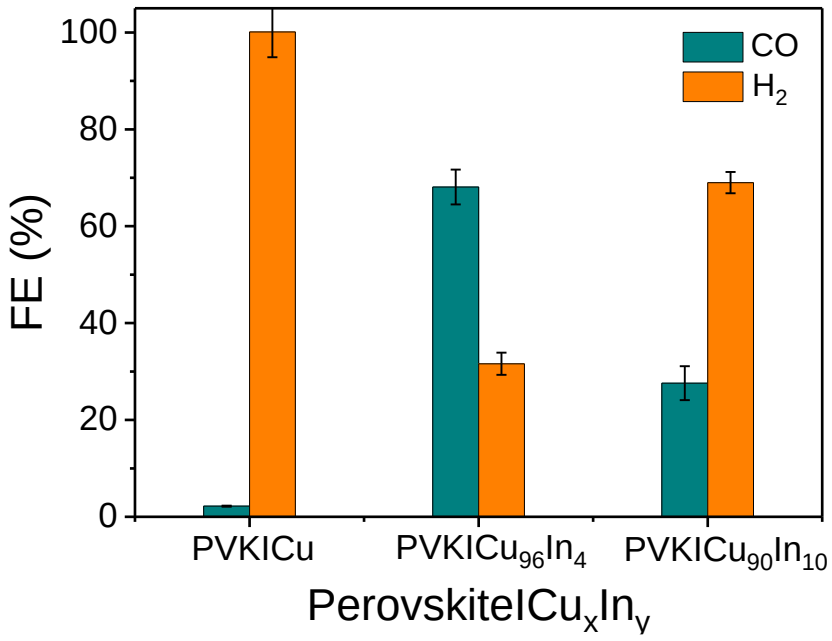

Fig. S10 Faradaic efficiency of products formed on buried perovskite-biased cathodes with different catalysts under 1 Sun illumination (chopped, 50 min on, 10 min off). Experiments were conducted in CO_2 saturated 0.5 M aqueous $KHCO_3$ (pH 7.2) at room temperature, the applied bias was +0.55 V vs RHE and the CPE duration was 4 h.

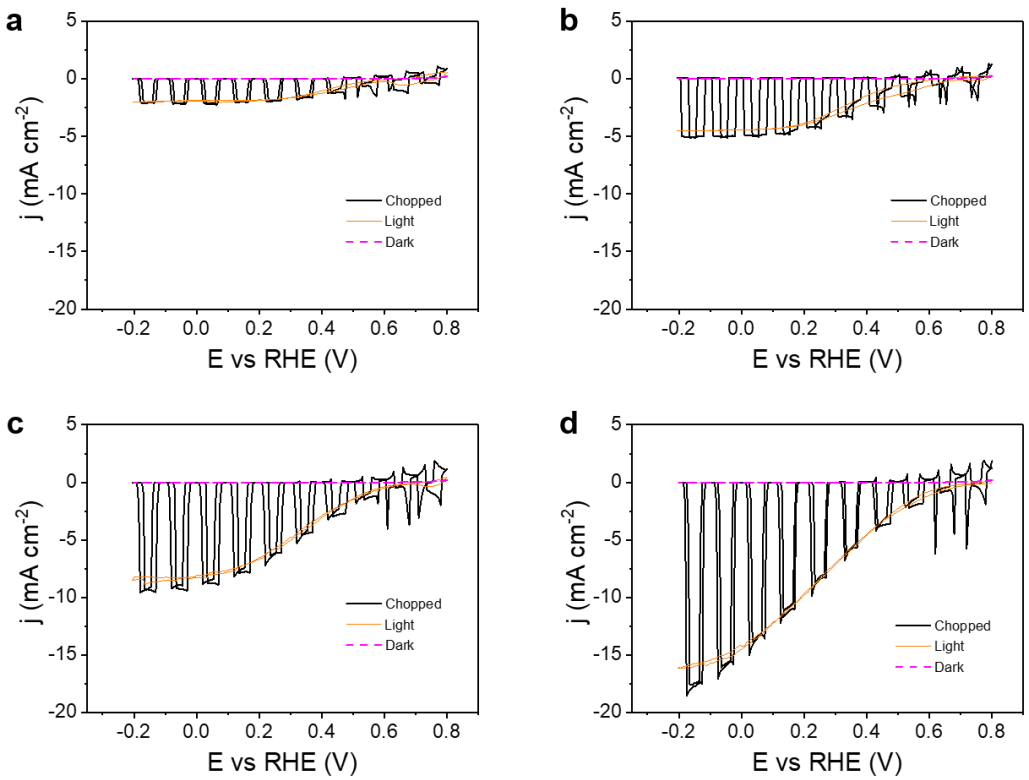

Fig. S11 PEC characterization of the perovskite|$Cu_{96}In_4$ cathodes under different light intensities: CV scans (chopped, continuous, and no illumination) under (a) 0.1, (b) 0.2, (c) 0.5 and (d) 1 Sun irradiation at room temperature. CO_2 saturated 0.5 M aqueous $KHCO_3$ (pH 7.2) was used as electrolyte solution. The scan rate was 10 mV s^{-1}.

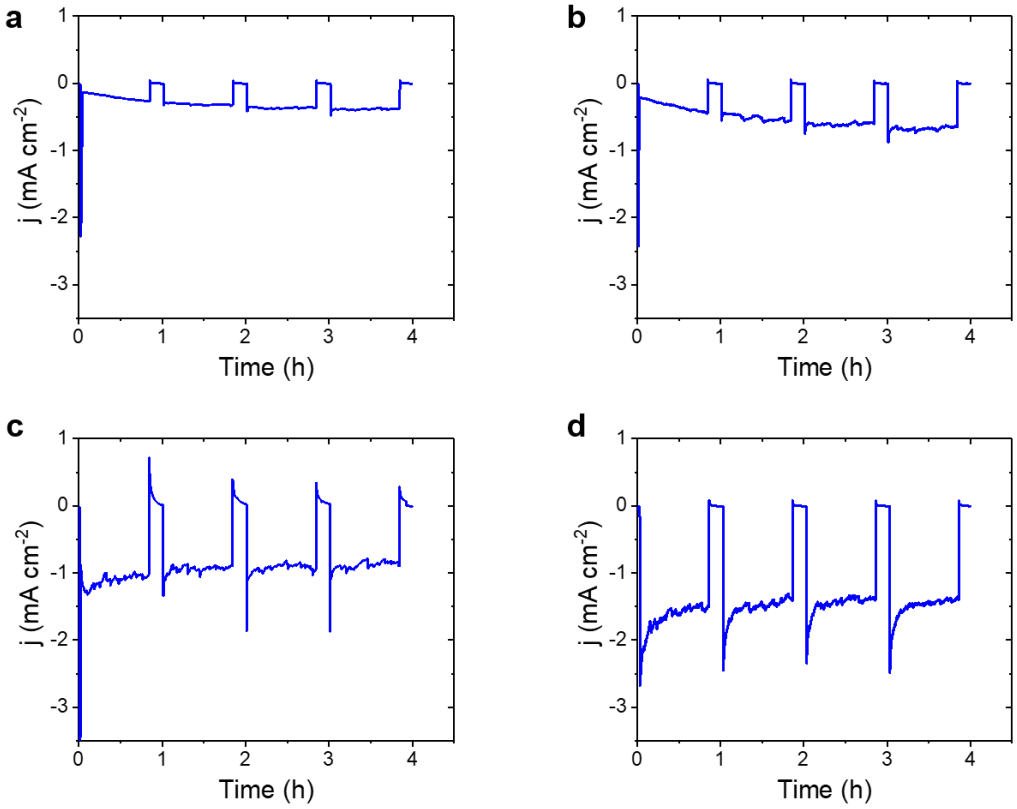

Fig. S12 PEC characterization of the perovskite|$Cu_{96}In_4$ cathodes using different simulated sunlight intensities: 4 h CPE under (a) 0.1, (b) 0.2, (c) 0.5 and (d) 1 Sun illumination showing the steady state photocurrent densities. The CPEs were performed under chopped light irradiation (50 min on, 10 min off) at +0.55 V vs RHE in CO_2 saturated 0.5M aqueous $KHCO_3$ (pH 7.2) at room temperature.

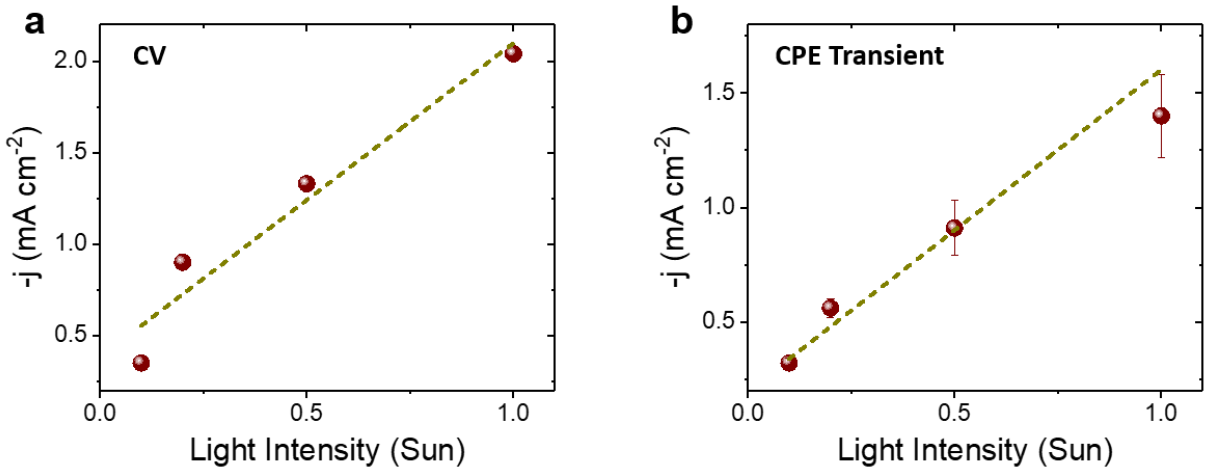

Fig. S13 Influence of light intensity on the buried perovskite-biased cathode performance: linear trend of photocurrents extracted from CVs (a) and CPEs (b) with the light intensity. The current values from the CVs are taken at +0.55 V vs RHE. Average steady-state photocurrents from the CPE triplicates are shown.

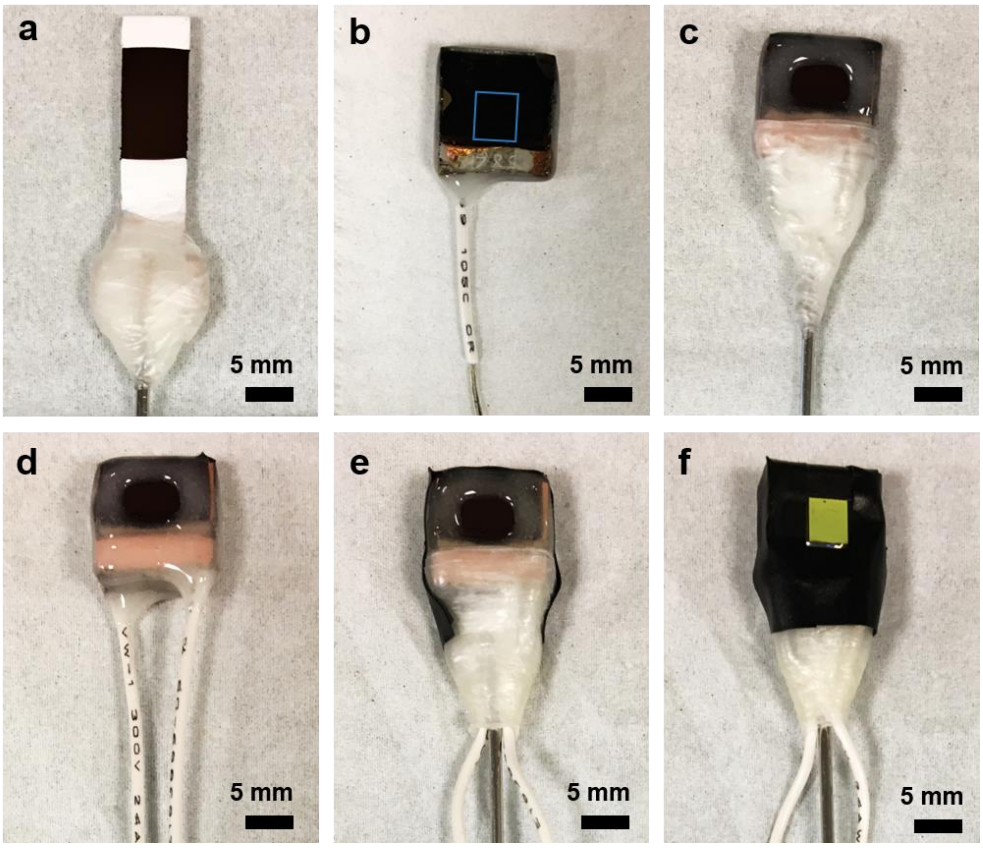

Fig. S14 Optical images of the catalyst and the PEC devices. (a) Cu_xIn_y catalyst on a Cu foil substrate, the electrode is attached to a metal rod with Parafilm for support. (b) Photograph of a perovskite film in a perovskite|Cu_xIn_y cathode from the backside where the active area is marked by a blue rectangle. (c) View from the catalyst side when the buried perovskite-biased cathode is attached to a metal rod support. A $BiVO_4$||perovskite|$Cu_{96}In_4$ tandem device before (d) and after (e,f) attaching to a metal rod support where (e) represents view from the catalyst side and (f) represents view from $BiVO_4$ side. Dark adhesive tape is used to cover the area surrounding the $BiVO_4$ to block excess light from reaching the perovskite active area.

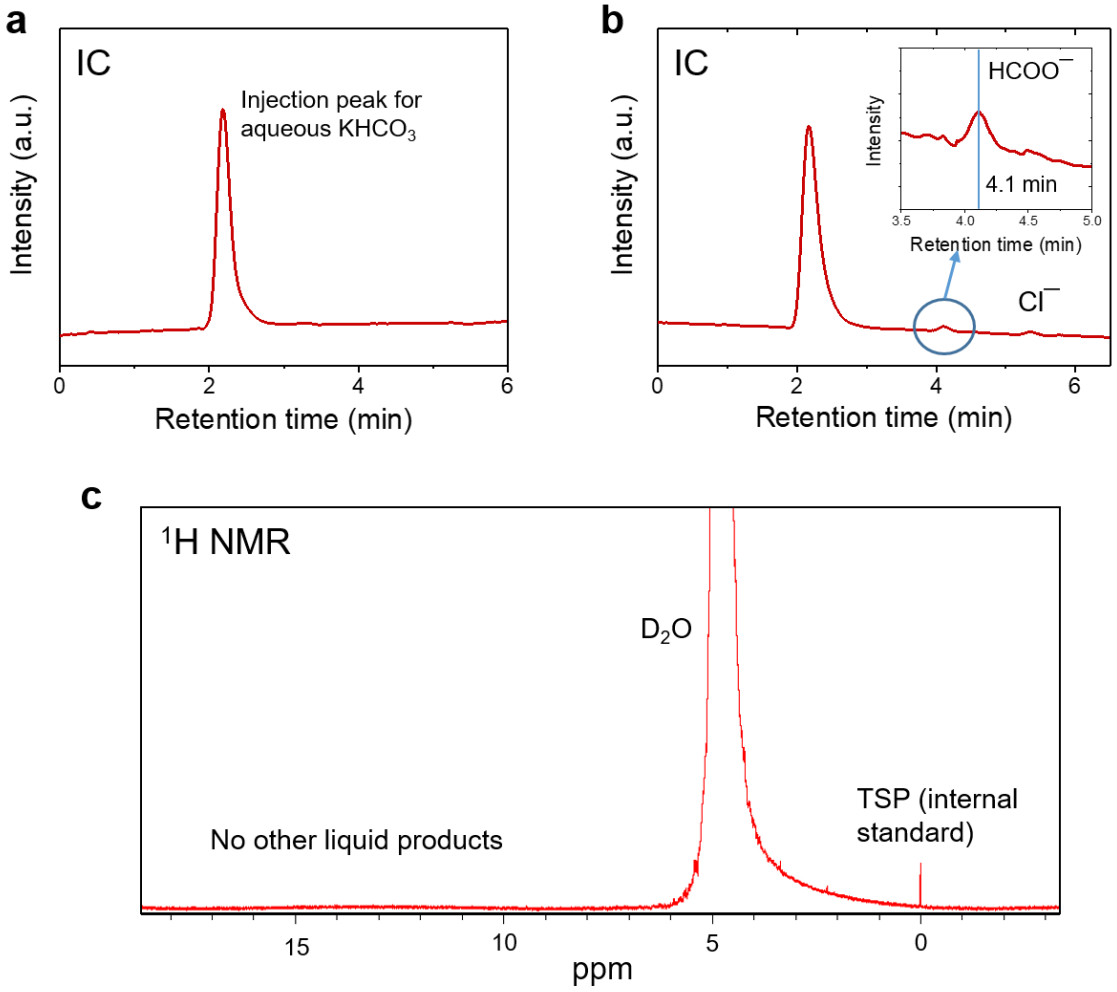

Fig. S15 Representative chromatograms and spectra of liquid product quantification by ion-exchange chromatography and ^{1}H NMR spectroscopy. (a) Chromatogram of 0.5 M aqueous $KHCO_3$ electrolyte showing the injection peak at around 2.2 min, (b) chromatogram and (c) ^{1}H NMR spectrum of liquid aliquot after 10 h photoelectrochemical experiments with the $BiVO_4$||perovskite|$Cu_{96}In_4$ tandem device under bias-free conditions. Sodium 3-(trimethylsilyl)propionate (TSP, 1mM) was used as the internal standard for ^{1}H NMR measurement in D_2O medium. Only a trace amount of formate was obtained as minor CO_2 reduction product.

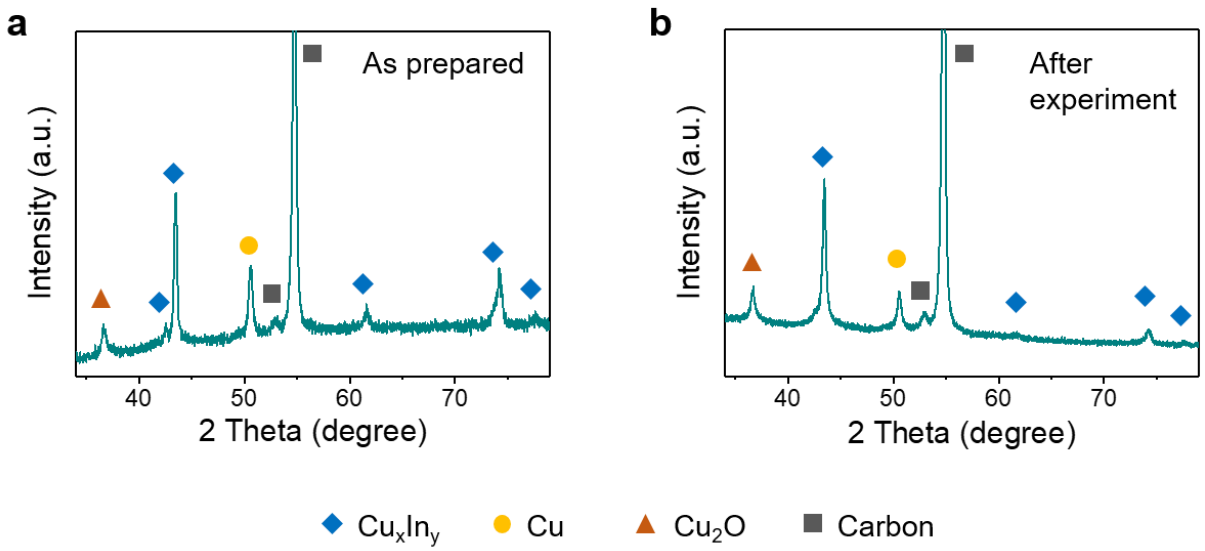

Fig. S16 XRD analysis of (a) as-prepared $Cu_{96}In_4$ alloy and (b) $Cu_{96}In_4$ alloy after a galvanostatic electrochemical experiment, where 200 µA cm^{-2} current density was applied for 500 min to mimic the tandem PEC experiment under bias free conditions by passing similar amount of charge. Some Cu_xIn_y facets have almost disappeared after the experiment due to agglomeration. The catalyst was deposited on a carbon foil substrate for the XRD analysis to avoid any substrate contribution. JCPDS 42-1476 and 35-1150 for Cu_xIn_y alloy, 85-1326 for Cu, and 75-1531 Cu_2O.

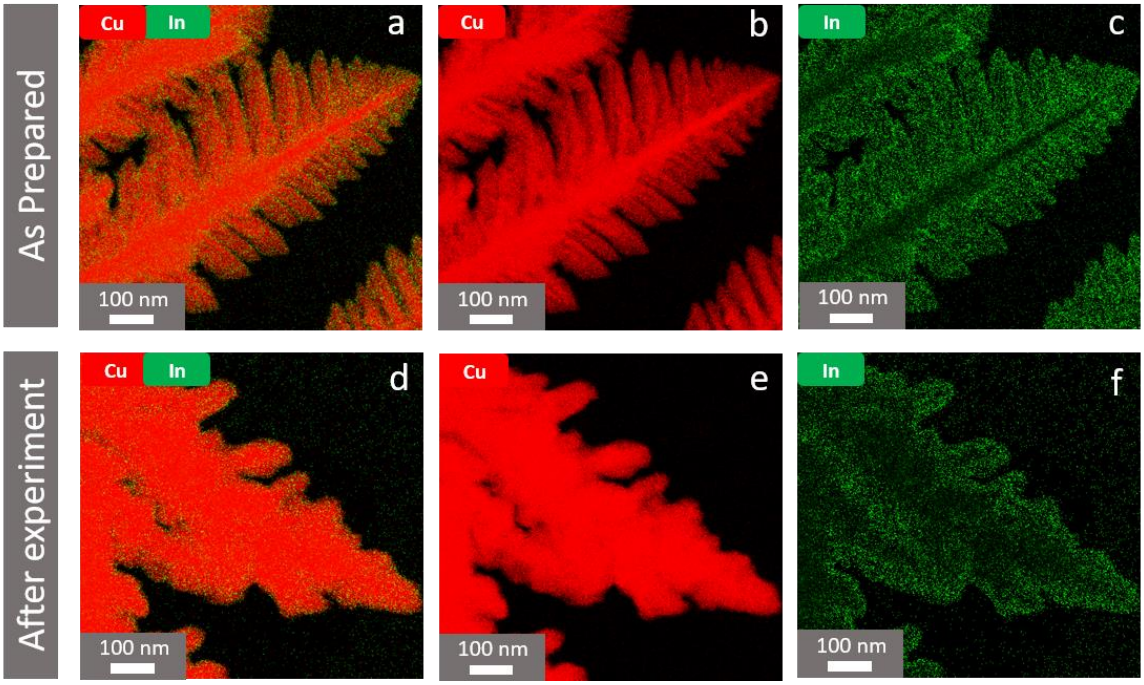

Fig. S17 High resolution STEM mapping of a single branch dendrite. (a-c) Elemental mapping of as prepared $Cu_{96}In_4$ catalyst showing a homogeneous distribution of Cu and In; (d-f) elemental mapping of the $Cu_{96}In_4$ catalyst after 10 h of photoelectrocatalysis under bias free conditions. It can be observed that some of the In phase separates out from the homogeneous CuIn phase during the experiment and accumulates along the periphery or, even migrates inside the bulk of the dendrites.

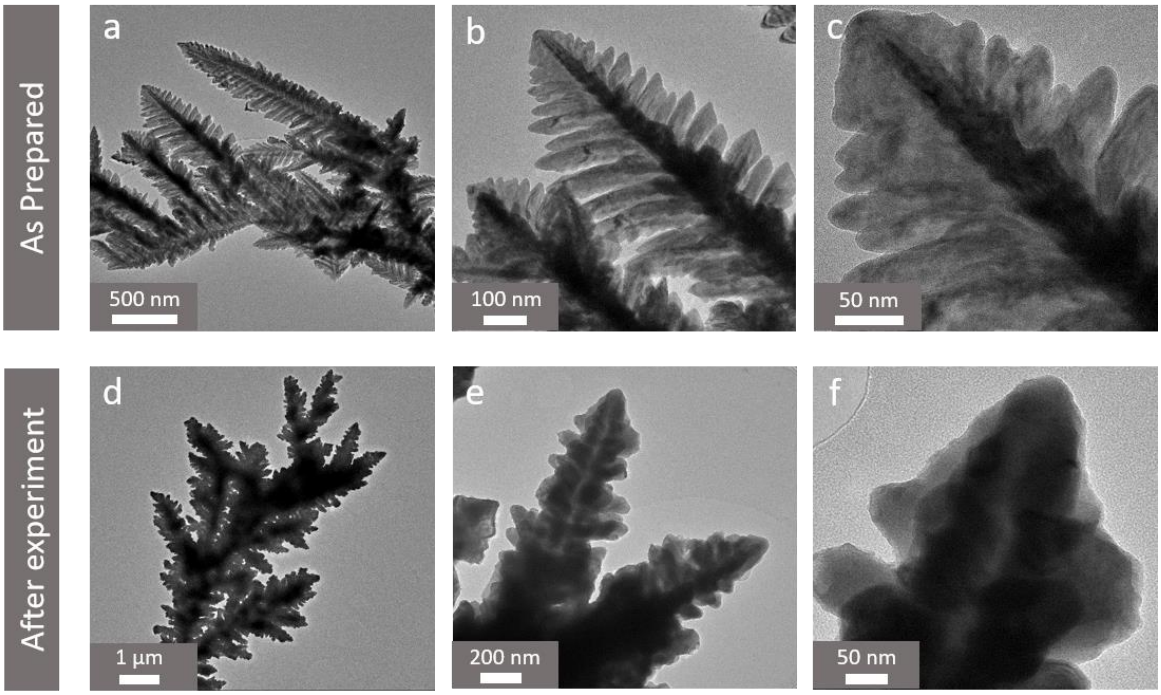

Fig. S18 TEM and HR-TEM analysis with (a-c) the as prepared $Cu_{96}In_4$ catalyst and (d-f) the catalyst after 10 h photo-electrolysis under bias free conditions. The dendritic structure stays intact after the experiment, indicating robustness of the catalyst. However, the nanostructures on the dendrites show some agglomeration after the experiment.

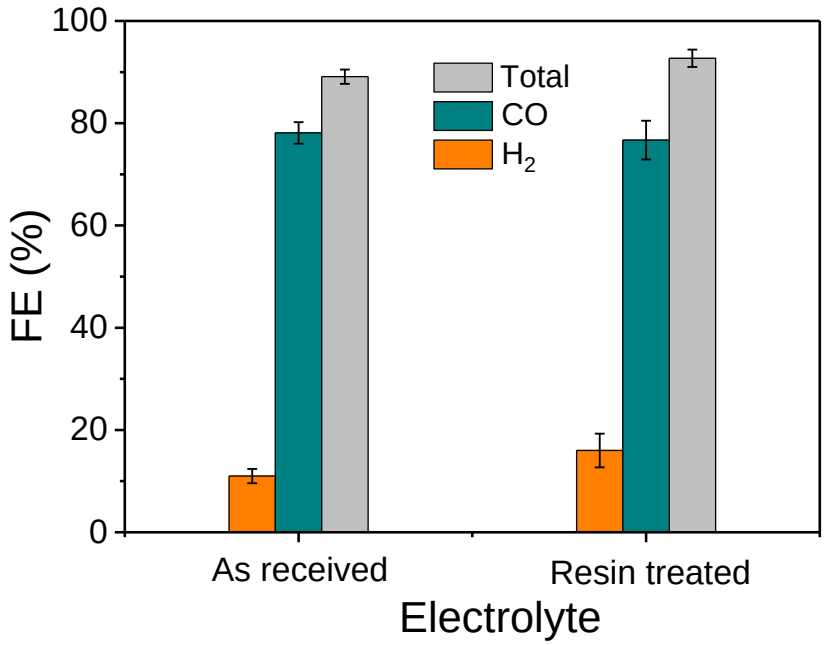

Fig. S19 Comparison of electrocatalytic activity of $Cu_{96}In_4$ catalyst in as-purchased 99.7% $KHCO_3$ electrolyte and in ultrapure resin treated 99.995% $KHCO_3$ electrolyte. The experiments were carried out for 4 h by applying -0.4 V vs RHE at room temperature. No significant change in catalytic activity of 3D porous $Cu_{96}In_4$ foam was observed in the ultrapure electrolyte.

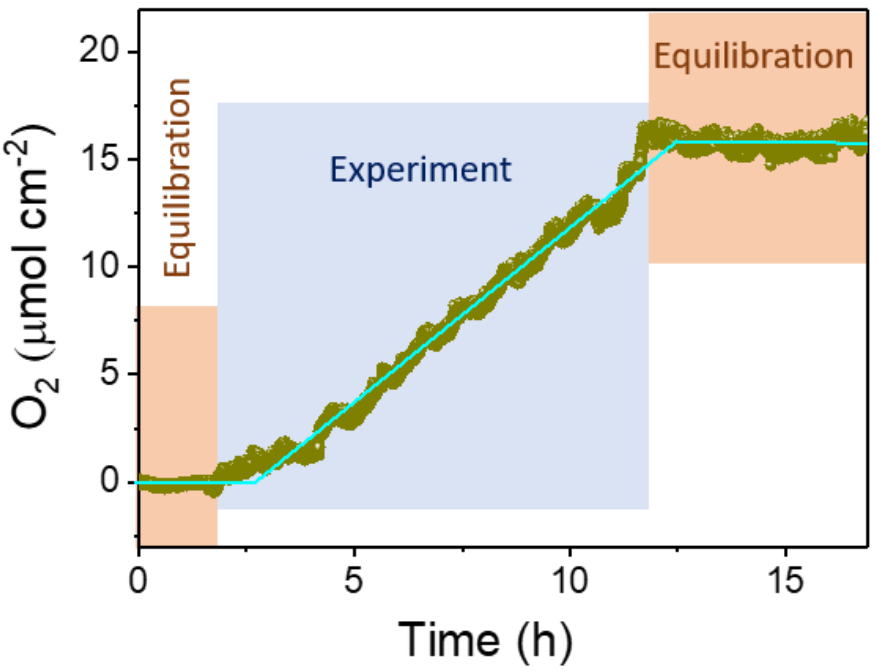

Fig. S20 Quantification of O_2 produced by the tandem device during the bias free CO_2 photoelectrocatalysis. The plot shows initial and final O_2 equilibration regions. The middle blue highlighted region accounts for the continuous increase in the O_2 amount during the bias-free experiment.

Supplementary Tables

Table S1. Numerical data: Potential dependent electrocatalytic performance of $Cu_{96}In_4$ electrode. Average faradaic efficiencies of CO and H_2 after 4 h CPE

E vs RHE (V)	FE_{CO} (%)	FE_{H2} (%)	FE_{Total} (%)
–0.3	71.2 ± 2.3	15.5 ± 4.4	86.7 ± 5.4
–0.4	78.1 ± 2.1	11.0 ± 1.4	89.1 ± 1.4
–0.5	74.3 ± 6.3	19.6 ± 6.8	93.9 ± 2.5
–0.6	73.8 ± 1.5	18.3 ± 3.9	92.1 ± 3.4

Table S2. Numerical data: Potential dependent electrocatalytic performance of $Cu_{96}In_4$ electrode. Average amounts of CO and H_2 after 4 h CPE.

E vs RHE (V)	n CO (μmol cm^{-2})	n H_2 (μmol cm^{-2})	n Total (μmol cm^{-2})
–0.3	15.40 ± 9.13	2.78 ± 1.22	18.18 ± 9.63
–0.4	38.01 ± 7.89	5.60 ± 1.97	43.61 ± 9.63
–0.5	75.53 ± 9.49	21.86 ± 11.7	97.39 ± 18.17
–0.6	128.80 ± 10.66	31.87 ± 6.34	160.67 ± 14.68

Table S3. Numerical data: Composition dependent electrocatalytic performance of Cu, $Cu_{96}In_4$, and $Cu_{90}In_{10}$ electrodes. Average faradaic efficiencies of CO and H_2 after 4 h CPE.

Electrode	FE_{CO} (%)	FE_{H2} (%)	FE_{Total} (%)
Cu	7.1 ± 1.0	77.0 ± 4.2	84.7 ± 3.1
$Cu_{96}In_4$	78.1 ± 2.1	11.0 ± 1.4	89.1 ± 1.4
$Cu_{90}In_{10}$	63.8 ± 4.6	25.4 ± 8.6	89.2 ± 5.1

Table S4. Numerical data: Composition dependent electrocatalytic performance of Cu, $Cu_{96}In_4$, and $Cu_{90}In_{10}$ electrodes. Average amounts of CO and H_2 after 4 h CPE.

Electrode	n CO (μmol cm^{-2})	n H_2 (μmol cm^{-2})	n Total (μmol cm^{-2})
Cu	2.47 ± 0.24	24.73 ± 2.44	27.2 ± 2.12
$Cu_{96}In_4$	38.01 ± 7.89	5.60 ± 1.97	43.61 ± 9.63
$Cu_{90}In_{10}$	17.01 ± 2.56	6.96 ± 2.61	23.97 ± 4.98

Table S5. Numerical data: Photoelectrocatalytic performances of different buried perovskite (PVK) cathodes containing Cu, $Cu_{96}In_4$, and $Cu_{90}In_{10}$ catalysts. Average amounts of CO and H_2 after 4 h CPE.

Perovskite cathode	n CO (μmol cm^{-2})	n H_2 (μmol cm^{-2})	n CO+H_2 (μmol cm^{-2})
PVK|Cu	1.5 ± 0.2	64.83 ± 11.5	66.33 ± 11.71
PVK|$Cu_{96}In_4$	52.78 ± 6.72	24.58 ± 4.69	77.40 ± 9.78
PVK|$Cu_{90}In_{10}$	19.96 ± 4.1	49.26 ± 3.3	69.22 ± 7.36

Table S6. Numerical data: Photoelectrocatalytic performances of different buried perovskite cathodes containing Cu, $Cu_{96}In_4$, and $Cu_{90}In_{10}$ catalysts. Average faradaic efficiencies of CO and H_2 after 4 h CPE.

Perovskite cathode	FE_{CO} (%)	FE_{H2} (%)	FE_{CO+H2} (%)
PVK|Cu	2.2 ± 0.1	100.1 ± 5.2	102.3 ± 4.6
PVK|$Cu_{96}In_4$	68.1 ± 3.6	31.6 ± 2.3	99.7 ± 2.8
PVK|$Cu_{90}In_{10}$	27.6 ± 3.5	69.0 ± 2.2	96.6 ± 2.5

Table S7. Numerical data: Photoelectrocatalytic performances of buried PVK|$Cu_{96}In_4$ cathodes under different light intensities. Average amounts of CO and H_2 after 4 h CPE.

Intensity (Sun)	n CO (μmol cm^{-2})	n H_2 (μmol cm^{-2})	n CO+H_2 (μmol cm^{-2})
0.1	12.53 ± 2.63	6.46 ± 0.69	18.99 ± 1.86
0.2	23.27 ± 2.1	11.12 ± 0.82	34.37 ± 1.39
0.5	38.45 ± 2.12	12.45 ± 3.58	50.90 ± 5.66
1	52.78 ± 6.72	24.58 ± 4.69	77.40 ± 9.78

Table S8. Numerical data: Photoelectrocatalytic performances of buried PVK|$Cu_{96}In_4$ cathodes under different light intensities. Average faradaic efficiencies of CO and H_2 after 4 h CPE.

Intensity (Sun)	FE_{CO} (%)	FE_{H2} (%)	FE_{CO+H2} (%)
0.1	61.5 ± 7.7	32.6 ± 5.5	94.1 ± 2.1
0.2	65.3 ± 3.6	31.5 ± 3.3	96.8 ± 3.6
0.5	70.1 ± 5.0	22.2 ± 4.4	92.3 ± 6.4
1	68.1 ± 3.6	31.6 ± 2.3	99.7 ± 2.8

Table S9. Bias free selective CO production from the tandem device: Average amount of CO, H_2 and O_2 produced during 10 h experiment.

Time (h)	n CO (μmol cm^{-2})	n H_2 (μmol cm^{-2})	n O_2 (μmol cm^{-2})
1	3.11 ± 0.18	0.28 ± 0.01	1.63 ± 0.65
2	5.87 ± 0.89	0.65 ± 0.1	2.89 ± 1.31
3	8.48 ± 1.16	1.14 ± 0.2	4.34 ± 0.84
4	10.84 ± 1.42	1.63 ± 0.27	6.12 ± 1.15
6	15.41 ± 2.04	3.07 ± 0.45	9.24 ± 1.63
8	18.58 ± 1.77	4.71 ± 0.66	12.26 ± 2.10
10	21.17 ± 2.04	7.21 ± 1.34	14.71 ± 3.15

Table S10. Bias free selective CO production from the tandem device: Average faradaic efficiencies of CO, H_2 and CO + H_2 produced during 10 h experiment.

Time (h)	FE_{CO} (%)	FE_{H2} (%)	FE_{CO+H2} (%)
1	71.7 ± 3.1	6.5 ± 0.2	78.2 ± 2.8
2	75.6 ± 3.5	8.4 ± 0.5	84 ± 4.0
3	77 ± 4.4	10.3 ± 1.0	87.3 ± 4.9
4	77.8 ± 3.5	11.7 ± 0.9	89.5 ± 4.3
6	80.5 ± 5.4	16 ± 1.9	96.5 ± 5.4
8	77.4 ± 1.2	19.6 ± 2.5	97 ± 3.7
10	72.5 ± 1.1	24.4 ± 2.7	96.9 ± 3.8

Supplementary References

1. H.-C. Shin and M. Liu, *Chem. Mater.*, 2004, **16**, 5460-5464.
2. A. Dutta, M. Rahaman, N. C. Luedi, M. Mohos and P. Broekmann, *ACS Catal.*, 2016, **6**, 3804-3814.
3. V. Andrei, R. L. Z. Hoye, M. Crespo-Quesada, M. Bajada, S. Ahmad, M. De Volder, R. Friend and E. Reisner, *Adv. Energy Mater.*, 2018, **8,** 1801403.
4. H. Lu, V. Andrei, K. J. Jenkinson, A. Regoutz, N. Li, C. E. Creissen, A. E. H. Wheatley, H. Hao, E. Reisner, D. S. Wright and S. D. Pike, *Adv. Mater.*, 2018, **30**, 1804033.
5. V. Andrei, K. Bethke and K. Rademann, *Phys. Chem. Chem. Phys.*, 2016, **18**, 10700-10707.
6. A. Wuttig and Y. Surendranath, *ACS Catal.*, 2015, **5**, 4479-4484.
7. M. Schreier, L. Curvat, F. Giordano, L. Steier, A. Abate, S. M. Zakeeruddin, J. Luo, M. T. Mayer and M. Grätzel, *Nat. Comm.*, 2015, **6**, 7326.
8. H. Dotan, N. Mathews, T. Hisatomi, M. Grätzel and A. Rothschild, *J. Phys. Chem. Lett.*, 2014, **5**, 3330-3334.

End of ESI